SANDIA REPORT
SAND2013-1749
Unlimited Release
Printed February 2013

Simulating Higher-Dimensional Geometries in GADRAS Using Approximate One-Dimensional Solutions

Gregory G. Thoreson, Dean J. Mitchell, and Lee T. Harding

Prepared by
Sandia National Laboratories
Albuquerque, New Mexico 87185 and Livermore, California 94550

Sandia National Laboratories is a multi-program laboratory managed and operated by Sandia Corporation, a wholly owned subsidiary of Lockheed Martin Corporation, for the U.S. Department of Energy's National Nuclear Security Administration under contract DE-AC04-94AL85000.

Approved for public release; further dissemination unlimited.

Issued by Sandia National Laboratories, operated for the United States Department of Energy by Sandia Corporation.

NOTICE: This report was prepared as an account of work sponsored by an agency of the United States Government. Neither the United States Government, nor any agency thereof, nor any of their employees, nor any of their contractors, subcontractors, or their employees, make any warranty, express or implied, or assume any legal liability or responsibility for the accuracy, completeness, or usefulness of any information, apparatus, product, or process disclosed, or represent that its use would not infringe privately owned rights. Reference herein to any specific commercial product, process, or service by trade name, trademark, manufacturer, or otherwise, does not necessarily constitute or imply its endorsement, recommendation, or favoring by the United States Government, any agency thereof, or any of their contractors or subcontractors. The views and opinions expressed herein do not necessarily state or reflect those of the United States Government, any agency thereof, or any of their contractors.

SAND2013-1749
Unlimited Release
Printed February 2013

Simulating Higher-Dimensional Geometries in GADRAS Using Approximate One-Dimensional Solutions

Gregory G. Thoreson, Dean J. Mitchell, and Lee T. Harding
Contraband Detection

Sandia National Laboratories
P.O. Box 5800
Albuquerque, New Mexico 87185-MS0782

ABSTRACT

The Gamma Detector Response and Analysis Software (GADRAS) software package is capable of simulating the radiation transport physics for one-dimensional models. Spherical shells are naturally one-dimensional, and have been the focus of development and benchmarking. However, some objects are not spherical in shape, such as cylinders and boxes. These are not one-dimensional. Simulating the radiation transport in two or three dimensions is unattractive because of the extra computation time required. To maintain computational efficiency, higher-dimensional geometries require approximations to simulate them in one-dimension. This report summarizes the theory behind these approximations, tests the theory against other simulations, and compares the results to experimental data. Based on the results, it is recommended that GADRAS users always attempt to approximate reality using spherical shells. However, if fissile material is present, it is imperative that the shape of the one-dimensional model matches the fissile material, including the use of slab and cylinder geometry.

CONTENTS

Figures 5
Tables 6
Nomenclature 7
Executive Summary 9
1 Introduction 11
2 Theory 13
2.1 Buckling Approximation 13
2.2 Point-Source Reduction Approximation 15
3 Results 19
3.1 Highly Enriched Uranium Tests 19
3.1.1 Neutron Multiplicity 20
3.1.2 Neutron Leakage 26
3.1.3 Photon Leakage 27
3.1.4 Multi-Layered Geometries 28
3.2 Comparison to Experimental Data 30
4 Conclusions 37
4.1 Recommendations for GADRAS Users 37
5 References 40
6 Distribution 41

FIGURES

Figure 1. Slab Source and Detector Geometry 15
Figure 2. Ratio of Detector Signal from Cosine-Angular-Distributed Slab to Uniform-Angular-Distributed Slab 16
Figure 3. Arbitrary Source Point and Circular Detector Geometry 17
Figure 4. Geometries tested include (a) slab configuration A, (b) slab configuration B, (c) slab configuration C, and (d) cylinder. The double hash marks indicate which dimensions of the object are equal. 19
Figure 5. Comparison of k_{eff} for Slab Configuration A 20
Figure 6. Percent Difference of 1-D and 2-D from 3-D Computed k_{eff} for Slab Configuration A 20
Figure 7. Percent Difference of 1-D/2-D/3-D from MC Computed k_{eff} for Slab Configuration A 21
Figure 8. Comparison of k_{eff} for Slab Configuration B 21
Figure 9. Percent Difference of 1-D and 2-D from 3-D Computed k_{eff} for Slab Configuration B 22
Figure 10. Percent Difference of 1-D/2-D/3-D from MC Computed k_{eff} for Slab Configuration B 22

Figure 11. Comparison of k_{eff} for Slab Configuration C 23
Figure 12. Percent Difference of 1-D and 2-D from 3-D Computed k_{eff} for Slab Configuration C 23
Figure 13. Percent Difference of 1-D/2-D/3-D from MC Computed k_{eff} for Slab Configuration C 24
Figure 14. Comparison of k_{eff} for Cylinder Geometry 24
Figure 15. Percent Difference of 1-D from 2-D Computed k_{eff} for Cylinder Geometry 25
Figure 16. Percent Difference of 1-D and 2-D from MC Computed k_{eff} for Cylinder Geometry 25
Figure 17. Average Error of Leakage Current between 1-D and Full-Dimensional Deterministic Models 26
Figure 18. Comparison of Leakage Current Computed by 1-D and 3-D Deterministic Models for a 15 cm Box 27
Figure 19. Average Error in Photon Leakage Current for Various Geometries Using the 1-D Approximation 28
Figure 20. Simulated Leakage Current from 1-D and 3-D Models Assuming Physical Dimensions of the Object for the Buckling Height and Width 29
Figure 21. Simulated Leakage Current from 1-D and 3-D Models Assuming Dimensions of the HEU Slab for the Buckling Height and Width 30
Figure 22. Simulated Photon Leakage Current from DU Plate 31
Figure 23. Simulated Photon Leakage Current from HEU Plate 31
Figure 24. Simulated Photon Leakage Current from Neptunium Cylinder 32
Figure 25. Comparison of Experimental (black), GADRAS-Simulated without Ray-tracing (red), and with Ray-tracing (green) HPGe Detector Signal from DU Plate 33
Figure 26. Comparison of Experimental (black), GADRAS-Simulated without Ray-tracing (red), and with Ray-tracing (green) HPGe Detector Signal from HEU Plate 33
Figure 27. Comparison of Experimental (black), GADRAS-Simulated without Ray-tracing (red), and with Ray-tracing (green) HPGe Detector Signal from Neptunium Cylinder 34
Figure 28. Comparison of Experimental (black), Simulated Sphere (red), Simulated Cylinder (green), and Simulated Slab (blue) for a 3 kg DU sphere measured with a HPGe detector 35

TABLES

Table 1. Comparison of keff and Leakage Current Error for 3-D and 1-D Simulations 29
Table 2. Reference for Selecting Appropriate Geometry 39

NOMENCLATURE

1-D	One-dimensional
2-D	Two-dimensional
3-D	Three-dimensional
DU	Depleted Uranium
ENSDF	Evaluated Nuclear Structure Data File
GADRAS	Gamma Detector Response and Analysis Software
HEU	Highly Enriched Uranium
HPGe	High-Purity Germanium
k_{eff}	K-effective, the eigenvalue of the transport solution
MC	Monte Carlo
MCNPX	Monte Carlo n-Particle eXtended (Software)
ONELD	One-Dimensional Linear Discontinuous (Software)
PARTISN	Parallel, Time-Dependent Sn (Software)
PE	Polyetheylene

EXECUTIVE SUMMARY

One-dimensional geometries, such as spheres, are attractive for modeling because the associated radiation transport calculations are solved quickly on personal computers. Spherical shells are one-dimensional because they can be described by only a single dimension, the radial position of the shells. Sometimes a real object is not well described by spherical shells, for example, cylinders are two-dimensional (2-D) objects and boxes are three-dimensional. While it is possible to model these higher dimensions explicitly, doing so increases the computation time by orders of magnitude, making its usefulness on a personal computer limited.

To circumvent this computational barrier, the buckling approximation is reviewed and a point-source-reduction approximation is developed. These approximations are applied to one-dimensional models to simulate them as two- or three-dimensional (3-D). This brings the result of the 1-D solution closer to the higher-dimensional solution while maintaining the computational efficiency.

The accuracy of buckling approximations are compared to higher-dimension simulations for highly enriched uranium (HEU) in various geometric configurations. The buckling approximation is able to match the criticality state computed by higher dimensions within 10% as long as the transverse dimensions (length and width for slabs, height for cylinders) are greater than a few mean-free-paths of the source neutron. The leakage from the geometry was compared to 3-D Monte Carlo n-Particle eXtended Software (MCNPX) simulations and experimental data. These approximations allowed the simulated leakage for depleted uranium (DU) plate, HEU plate, and neptunium cylinder to match the MCNPX simulated data well. The experimental data compared well for the DU and HEU plates, but not for the neptunium cylinder. It is unclear whether there is experimental error, or an error in the approximation.

Overall, the ability of these approximations to simulate higher-dimensional geometries using one-dimensional approximations is good. It is advisable to GADRAS users, however, to approximate reality using spherical shells whenever possible. Only when fissile material is present in the shape of a slab or cylinder should a user utilize these higher-dimensional geometries. A list of recommendations and advice for modeling higher-dimensional geometries is found in the conclusion section of this document.

1 INTRODUCTION

In addition to a rich library of neutron and gamma detector responses, the software package Gamma Detector Response and Analysis Software (GADRAS) is capable of simulating sources utilizing deterministic radiation transport routines. Efficient radiation transport calculations are crucial as the inverse problem solver in GADRAS requires sequential solutions to converge. This approach relies on one-dimensional (1-D) deterministic radiation transport solutions, which are computationally efficient compared to 2-D or 3-D deterministic or Monte Carlo (MC) calculations.

Because spherical objects naturally have polar and azimuthal symmetry, it is convenient and often accurate to model many problems as spherical shells. Even geometries that are not spherical in nature can be modeled as such if the materials within the line-of-sight from the source to the detector are placed in spherical shells, with the thickness of each shell equal to the distance traversed in that material. However, for some geometries this approximation is not valid. An example of a problematic geometry is nuclear reactor plate fuel. This slab-type geometry is inherently a 3-D problem. With sufficient source-to-detector distance the plate may be reduced to a point source and the spherical approximation for intervening materials may work well. However, the estimation of the source strength is reliant on the multiplication of the system, which must be modeled in this higher-dimensional geometry. To maintain the efficiency of the radiation transport, efforts are made to approximate 3-D slab geometries in 1-D. This report reviews the theory and validity of these approximations in a variety of geometric configurations by comparing simulated and experimental data.

2 THEORY

2.1 Buckling Approximation

The well-established diffusion approximation to the time-independent Boltzmann transport equation for all energies is given by

$$-\mathrm{D}\nabla^2\phi + \sigma_a\phi = \frac{1}{k}\nu\sigma_f\phi, \tag{1}$$

where D is the diffusion coefficient given by $1/3\sigma_{tr}$ and σ_{tr} is the transport cross-section (all cross sections are in units of $[cm^{-1}]$). By defining the buckling term as

$$B^2 = \frac{\frac{\nu\sigma_f}{k} - \sigma_a}{D}, \tag{2}$$

Equation (1) may be re-written as

$$-\nabla^2\phi = B^2\phi. \tag{3}$$

In one dimension (slab geometry), the solution to Equation (3) is

$$\phi = \phi_0 \cos(xB). \tag{4}$$

For a slab of width d $[cm]$ in a vacuum, diffusion theory states that the flux must go to zero at the extrapolation distance. Therefore the buckling is equal to

$$B = \frac{\pi}{d + 2\delta}, \tag{5}$$

where δ is the extrapolation distance in $[cm]$ given by $0.7104/\sigma_{tr}$. For a highly scattering material, σ_{tr} may be approximated with σ_t. This is known as the geometric buckling term. By substituting Equation (3) into Equation (1) and integrating over the domain of the problem, the transport equation may be re-written as the following balance equation:

$$\{Leakage\} + \{Absorption\} = \{Sources\}$$
$$\left\{\int DB^2\phi\, dx\right\} + \left\{\int \sigma_a\phi\, dx\right\} = \left\{\int \frac{1}{k}\nu\sigma_f\phi\, dx\right\} \tag{6}$$
$$\int (\sigma_a + DB^2)\phi\, dx = \int \frac{1}{k}\nu\sigma_f\phi\, dx$$

If the problem domain is infinite, there is no leakage and the DB^2 term goes to zero. Thus, an alternative formulation to explicitly modeling leakage is to treat the source as if it had infinite extent, and approximate the leakage in the system by augmenting the absorption cross section by a factor of DB^2, utilizing the geometric buckling defined in Equation (5). This is known as a *buckling correction.*

This argument is easily extendible to higher dimensions as the buckling term for a two-dimensional slab with dimensions x and y is

$$B^2 = \left(\frac{\pi}{x + 2\delta}\right)^2 + \left(\frac{\pi}{y + 2\delta}\right)^2, \tag{7}$$

Thus, a 3-D slab with dimensions x, y, z $[cm]$ may be approximated by explicitly modeling the x-dimension and approximating leakage in the transverse directions by introducing a buckling absorption cross section equal to

$$\sigma_b = DB^2,$$
$$\sigma_b = \frac{1}{3\sigma_{tr}}\left[\left(\frac{\pi}{y + 2\delta}\right)^2 + \left(\frac{\pi}{z + 2\delta}\right)^2\right], \tag{7}$$
$$\sigma_b = \frac{\sigma_{tr}}{3}\left[\left(\frac{\pi}{\sigma_{tr}y + 1.4209}\right)^2 + \left(\frac{\pi}{\sigma_{tr}z + 1.4209}\right)^2\right],$$

and augmenting the absorption cross section by this amount throughout the entire domain. The buckling correction in the axial dimension for cylinders is very similar, given by

$$\sigma_b = \frac{\sigma_{tr}}{3}\left(\frac{\pi}{\sigma_{tr}z + 1.4209}\right)^2, \tag{8}$$

where z is the height of the cylinder.

The validity of this approximation hinges on diffusion theory. The accuracy of the diffusion approximation becomes worse in highly absorbing media, near boundaries or material interfaces, and in highly anisotropic scattering systems. Nevertheless, it remains a convenient alternative to explicitly modeling 3-D geometries.

2.2 Point-Source Reduction Approximation

In order to maintain consistency with the way GADRAS processes radiation leakage from sources that are modeled as spheres, we reduce the leakage from slabs and cylinders to produce equivalent point sources emitting radiation into 4π. There are two obstacles with higher-dimensional geometries that must be overcome to achieve this equivalence: (1) the leakage that is relevant to the detector response pertains to a single facet of the geometry, and (2) the angular distribution on the surface of the object affects the probability that the radiation will strike the detector.

For slab geometries, GADRAS imposes symmetry about the origin. Thus, the leakages from both sides of the slab are equal. The leakage out the front face only needs to be doubled to account for the leakage out the back side, which is not included in the discrete ordinates calculation. However, like the top and bottom of the cylinder, there is no information regarding the leakage from the other four sides of the slab. A simple approximation is made that the leakage per unit area from the other facets is equal to the leakage per unit area from the facet computed. This is a valid approximation as long as the slab's thickness is much less than the length and width, and the cylinder's height is much larger than its radius.

The second problem regarding the angular distribution is more complicated. In Figure 1, the angular distribution of the current on the surface of a slab is depicted by the length of red arrows emanating from a point on the surface. On the surface of any geometry, the angular distribution of the current cannot be isotropic. For the particle flux to be finite, the current parallel to the surface must go to zero. Let θ be the angle between the surface normal $\hat{n}$ and the angular current. The probability distribution function of the current can be represented according to a cosine distribution,

$$p(\theta)d\theta = cos^n\theta \, d\theta$$

where $n \in [0, \infty)$ is the power of the cosine distribution. For finite slab geometries, this non-uniform distribution causes the source to be "beam-like" as opposed to isotropic, which increases the probability of incidence on the detector face for a detector that is normal to the plane of the slab.

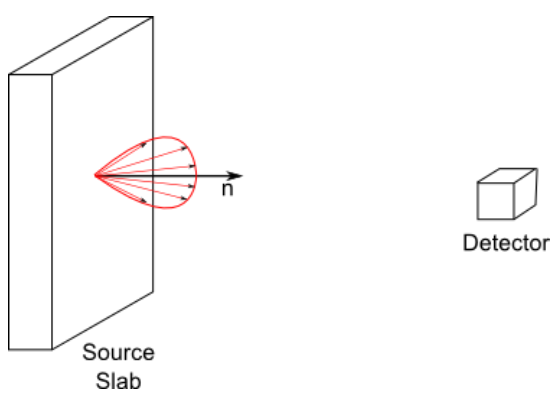

Figure 1. Slab Source and Detector Geometry

The angular distribution on the surface of any geometry may be ignored in a few special cases:

1) **Small spheres** – if the radius of the sphere is much less than the distance to the detector, the angular distribution is irrelevant as any increased contribution on one point of the sphere is exactly cancelled out by a decreased contribution from another point on the sphere.
2) **Large slabs** – as the length and width of the slab approach infinity, the angular distribution can be ignored. This observation is especially important for terrestrial background calculations, where the ground is essentially an infinite plane. Consider a detector 1 meter away from a slab of varying extent (length and width). The ratio of the detection probability of particles exiting the slab with cosine-power angular distribution to the detection probability of particles exiting with a uniform angular distribution is plotted in Figure 2 for varying degrees of cosine power, n. Clearly, as the slab approaches infinity, the ratios converge to unity regardless of cosine power.

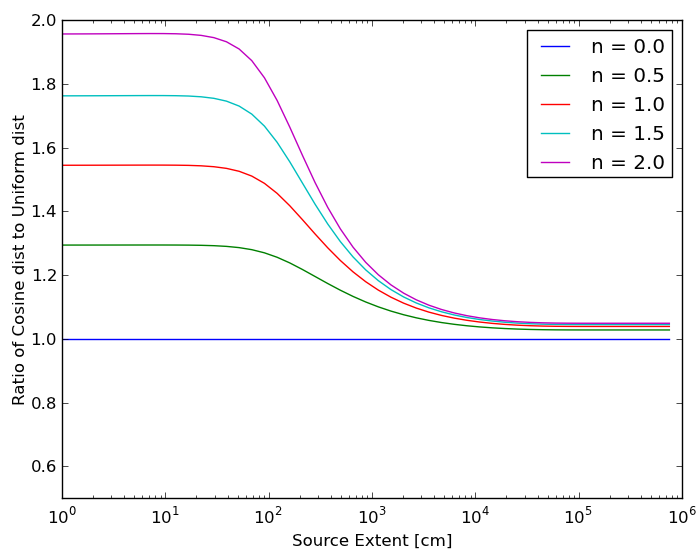

Figure 2. Ratio of Detector Signal from Cosine-Angular-Distributed Slab to Uniform-Angular-Distributed Slab

3) **Tall cylinders** – the angular distribution can be ignored for very tall cylinders. Like the slab, as the cylinder's extent approaches infinity, the increased contribution from the non-uniform angular distribution at the center of the cylinder is exactly cancelled by a decrease in contribution from points away from the center.

Except for these three special cases, the angular distribution for the emitted radiation may be important. A correction can be applied by computing the ratio of the cosine-distributed surface to the uniformly-distributed surface. Consider Figure 3, which has a point in space $\vec{s}$ on a surface with normal $\hat{n}_s$ and a detector circle centered at $\vec{d}$ with radius R and normal $\hat{n}_d$. The source

surface normal is projected onto the detector-circle-plane. This projected line is extended to the edges of the detector to points $\vec{p}_1$ and $\vec{p}_2$. The angles between vector $(\vec{p}_1 - \vec{s})$ and $\hat{n}_s$, and between $(\vec{p}_2 - \vec{s})$ and $\hat{n}_s$ are computed as θ_1 and θ_2, respectively. These two angles define the edges of the detector in the polar angle dimension.

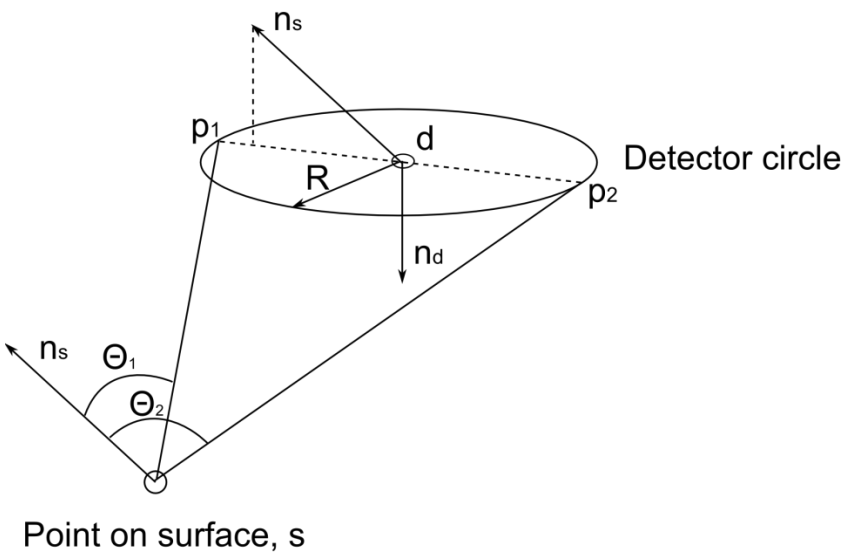

Figure 3. Arbitrary Source Point and Circular Detector Geometry

With the polar angle limits defined in this way, it is possible to compute the relative probability that a cosine-distributed source from this point on the surface will strike the detector versus a uniformly-distributed source. First, the probability of being emitted into this polar angle region is

$$p = \frac{\int_{\theta_1}^{\theta_2} cos^n\,\theta\,d\theta}{\int_0^{\pi/2} cos^n\,\theta\,d\theta} \tag{9}$$

The same probability for a uniform source is

$$p^{uniform} = \frac{2(\theta_2 - \theta_1)}{\pi} \tag{10}$$

Thus, the ratio of the two probabilities, F, is

$$F = \frac{\pi}{2(\theta_2 - \theta_1)} \frac{\int_{\theta_1}^{\theta_2} cos^n\,\theta\,d\theta}{\int_0^{\pi/2} cos^n\,\theta\,d\theta} \tag{11}$$

There is a closed form solution to this integral using the hyper-geometric function, but its complexity makes a simple numerical integration technique more attractive. This formula for F is the appropriate scaling factor for a single point on the surface. By meshing the slab, cylinder, or sphere with evenly spaced points, this formula may be repeated and the results averaged to determine the appropriate scaling factor for the entire surface. This approximation only integrates over the polar angle dimension and assumes uniformity in the azimuth. An exact formulation would integrate over the solid angle subtended by the detector, including the azimuthal dimension. However, the detector may not be circular, and the relative minor variation in the width of the azimuth as a function of polar angle only introduces a small error.

The cosine power, n, required for these equations is computed by calculating the angular current from the angular flux at the outer surface of the geometry. The angular current data is fit with a cosine distribution function using a simple gradient-descent optimization algorithm. The computed cosine power is output to GADRAS' ".gam" files as the fourth entry on the first line.

The area-scaling is done prior to creation of the ".gam" file. Therefore, the ".gam" file contains the total output from all sides of the object. Because the angular-distribution-scaling is dependent on the detector geometry, it is done after the ".gam" file is read, utilizing the fourth entry in the ".gam" file as the cosine power.

3 RESULTS

The buckling approximation is tested by comparing results from Parallel, Time-Dependent Sn Software (PARTISN) [1] and MCNPX [2] and One-Dimensional Linear Discontinuous Software (ONELD) [3]. PARTISN is a 1-D/2-D/3-D discrete ordinates deterministic transport code which has buckling correction options built-in for 1-D and 2-D geometries. It is used as the deterministic neutron transport solver. MCNPX is a 3-D Monte Carlo transport code. It is used as the Monte Carlo neutron and photon transport solver. ONELD is a 1-D discrete ordinates deterministic code and is used as the deterministic photon solver. GADRAS utilizes PARTISN and ONELD in 1-D to simulate the neutron, photon, and electron transport. Thus, utilizing these tools directly to examine the accuracy of the buckling correction is appropriate to determine GADRAS' capabilities.

3.1 Highly Enriched Uranium Tests

The test problem is a slab and cylinder of highly enriched uranium (HEU) (93.5% enriched, aged 20 years), with variable dimensions. The slab geometry is subdivided into three aspect ratios as illustrated in Figure 4.

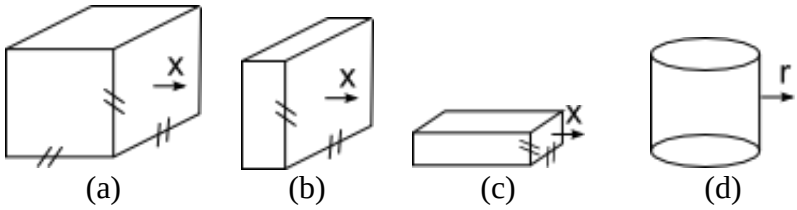

Figure 4. Geometries tested include (a) slab configuration A, (b) slab configuration B, (c) slab configuration C, and (d) cylinder. The double hash marks indicate which dimensions of the object are equal.

The characteristic dimension of each object is taken to be the variable dimension. This dimension is varied from 1 cm to 15 cm. For configuration A, all three dimensions are varied simultaneously. For configuration B, the x-dimension is fixed at 1 cm while the other two dimensions are varied simultaneously. For configuration C, the x-dimension is fixed at 15 cm while the other two dimensions are varied simultaneously. For the cylinder, the height is fixed at 15 cm while the diameter is varied from 1 to 15 cm. Results from neutron (PARTISN/MCNPX) and photon (ONELD/MCNPX) transport simulations are compared. While the buckling correction does not affect the photon results as strongly as the neutron, it is included for completeness. For neutrons, two comparison metrics are considered in this evaluation: the calculated k-effective (k_{eff}), and the leakage in the positive x-direction (or r-direction for cylinders). For photons, only the leakage is compared for the HEU tests. In addition, the effect of multiple layers in three dimensions is examined.

3.1.1 Neutron Multiplicity

The k_{eff} as computed by PARTISN in (1-D/2-D/3-D) and MCNPX (MC) is compared in Figure 5 through Figure 16. The 1-D and 2-D simulations utilize the buckling correction. In all MC simulations, the relative statistical uncertainty on the k_{eff} estimate is less than 0.1%.

3.1.1.1 Slab Configuration A k_{eff} Comparison

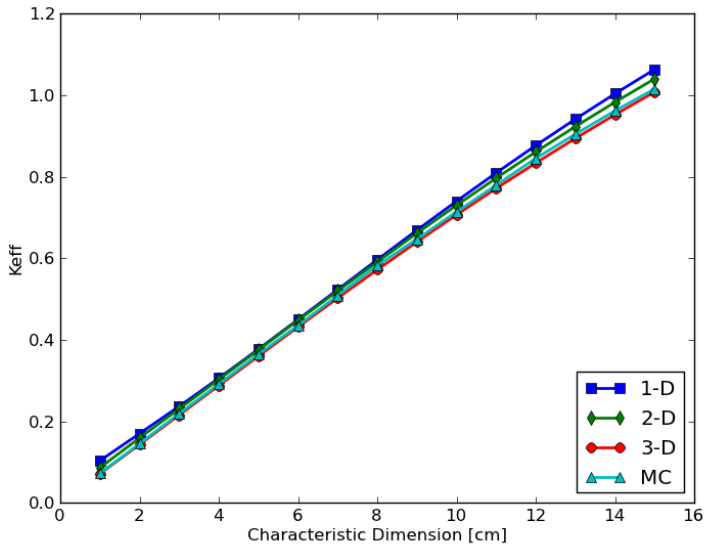

Figure 5. Comparison of k_{eff} for Slab Configuration A

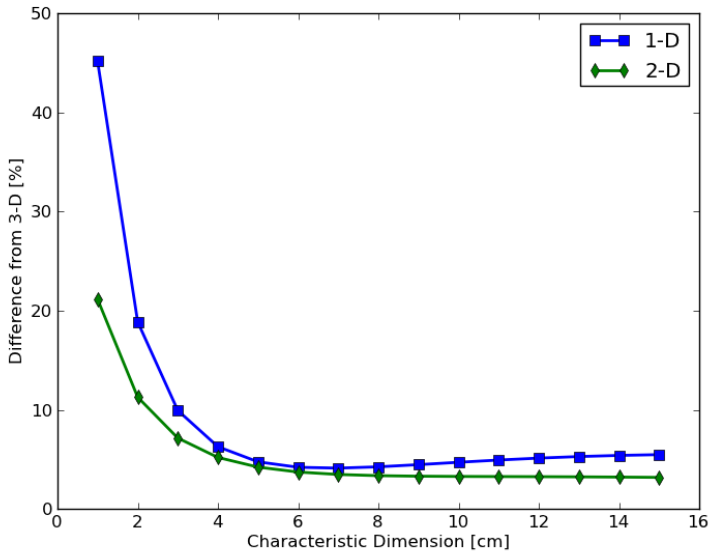

Figure 6. Percent Difference of 1-D and 2-D from 3-D Computed k_{eff} for Slab Configuration A

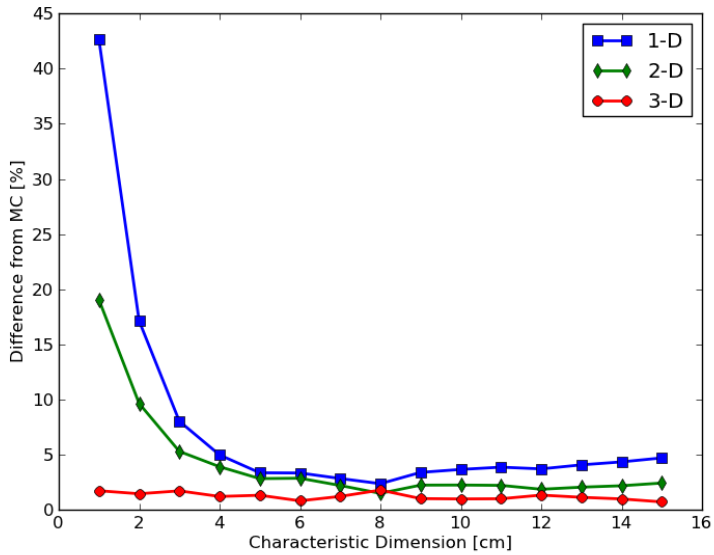

Figure 7. Percent Difference of 1-D/2-D/3-D from MC Computed k_{eff} for Slab Configuration A

3.1.1.2 Slab Configuration B k_{eff} Comparison

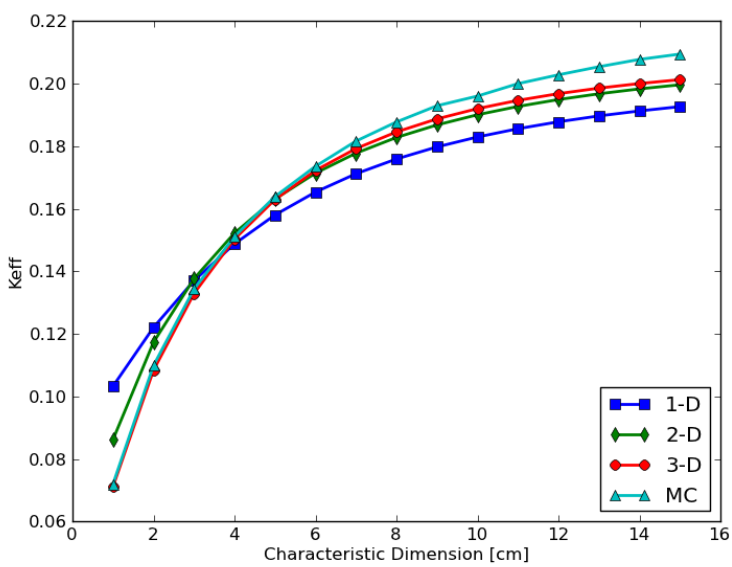

Figure 8. Comparison of k_{eff} for Slab Configuration B

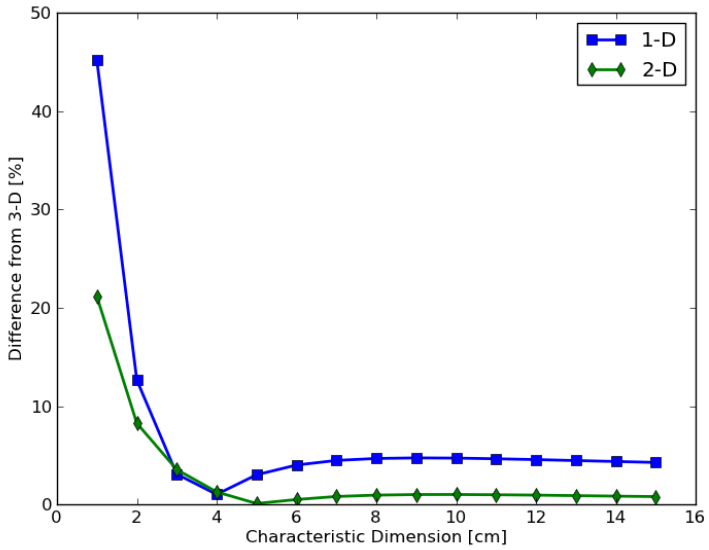

Figure 9. Percent Difference of 1-D and 2-D from 3-D Computed k_{eff} for Slab Configuration B

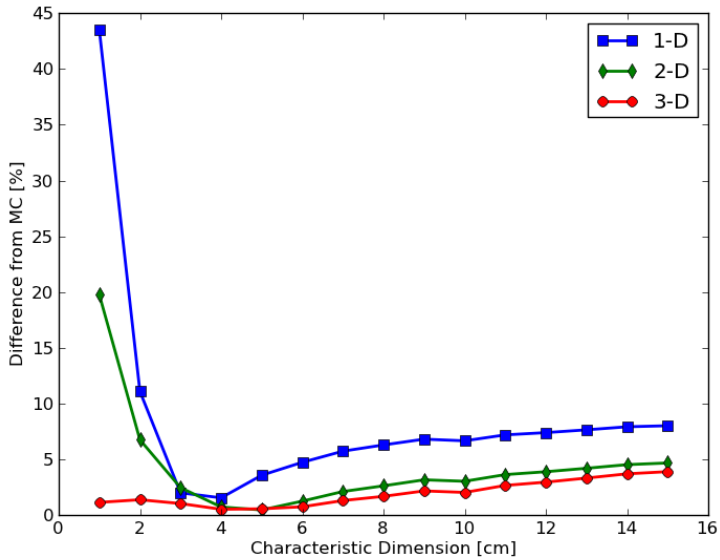

Figure 10. Percent Difference of 1-D/2-D/3-D from MC Computed k_{eff} for Slab Configuration B

3.1.1.3 Slab Configuration C k_{eff} Comparison

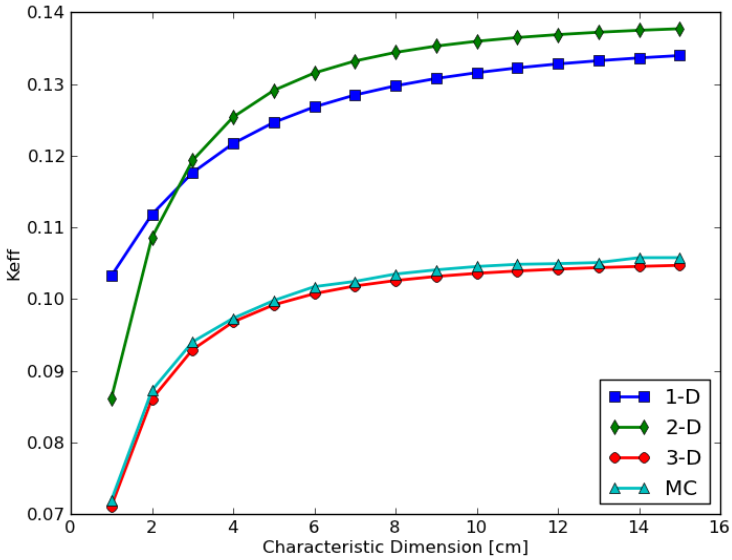

Figure 11. Comparison of k_{eff} for Slab Configuration C

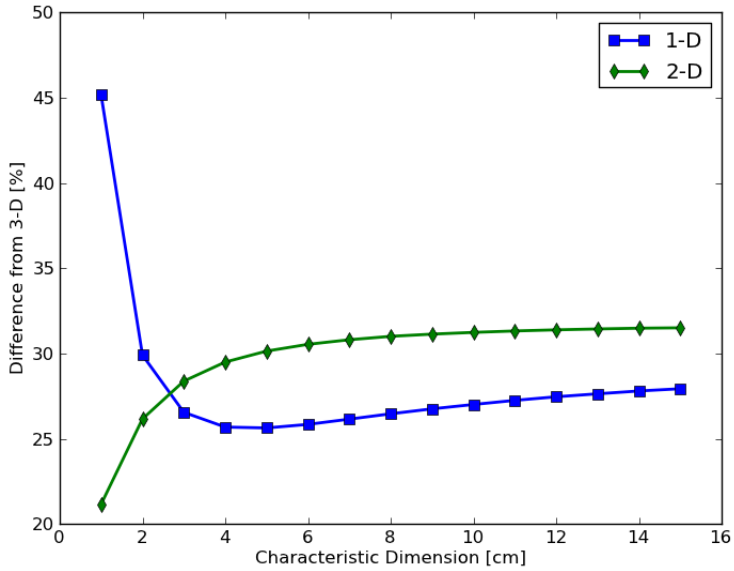

Figure 12. Percent Difference of 1-D and 2-D from 3-D Computed k_{eff} for Slab Configuration C

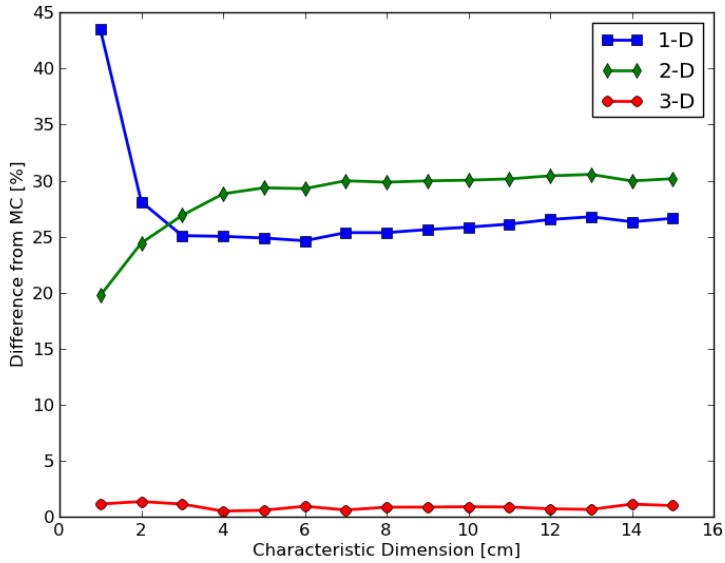

Figure 13. Percent Difference of 1-D/2-D/3-D from MC Computed k_{eff} for Slab Configuration C

3.1.1.4 Cylinder k_{eff} Comparison

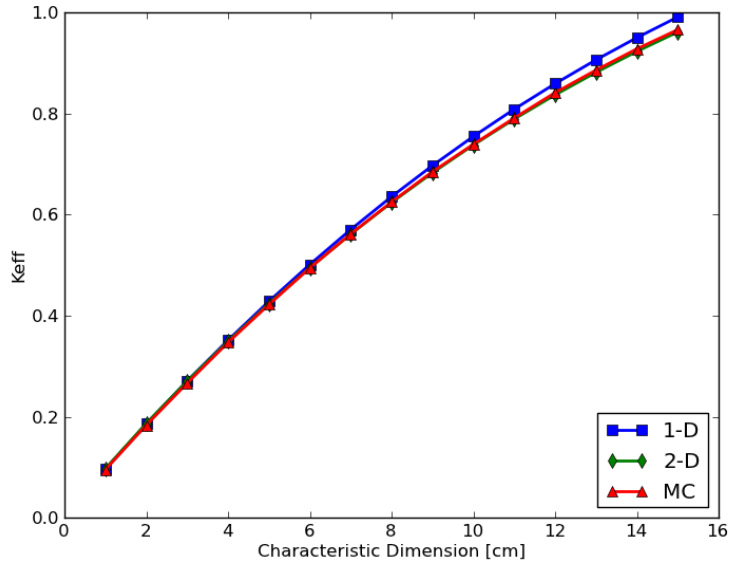

Figure 14. Comparison of k_{eff} for Cylinder Geometry

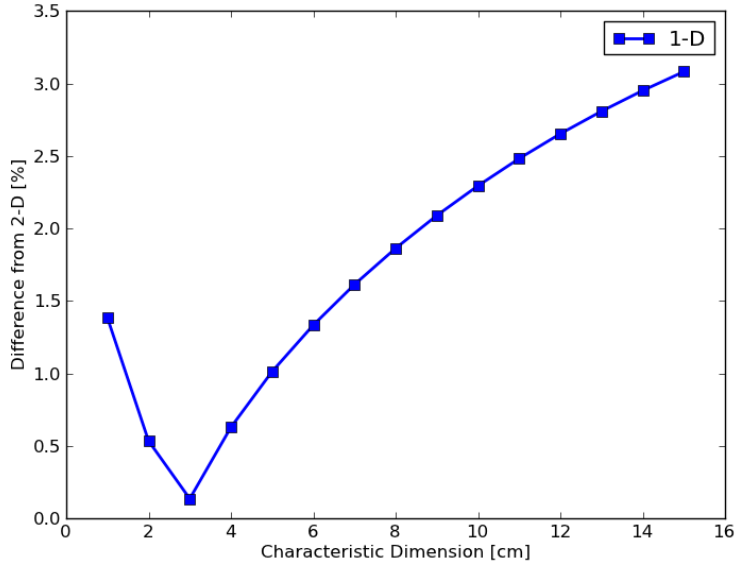

Figure 15. Percent Difference of 1-D from 2-D Computed k_{eff} for Cylinder Geometry

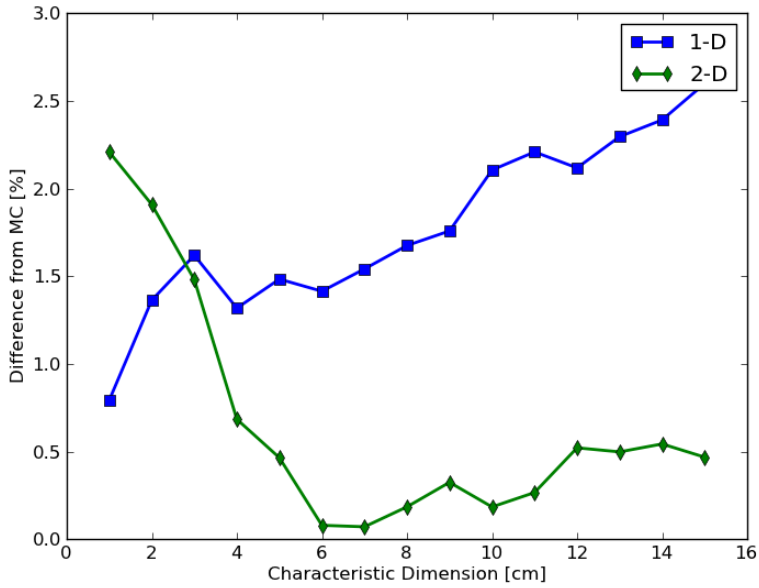

Figure 16. Percent Difference of 1-D and 2-D from MC Computed k_{eff} for Cylinder Geometry

The good agreement between the 3-D and MC simulations indicate that the PARTISN and MCNPX solvers are calculating a reasonable k_{eff} from their respective cross-section libraries and transport routines. The k_{eff} as computed by the 1-D and 3-D simulations are comparable for objects greater than a few centimeters in size, except for slab configuration C geometry. The approximation on cylindrical geometry has good agreement for all dimensions of the cylinder.

3.1.2 Neutron Leakage

Based on the good agreement between the full-dimensional deterministic and the Monte Carlo simulations, the leakage out the "front face" (x-dimension for Cartesian, r-dimension for cylindrical) of each of the geometries is compared in 1-D versus the full-dimension (3-D for Cartesian, 2-D for cylindrical), which is taken as the "true" answer. Furthermore, achieving reasonable uncertainties for low probability events, such as a thermal neutron leaking from the system, is a difficult feat using Monte Carlo techniques. Comparing the deterministic results grants a full-spectrum comparison.

The average difference between 1-D and 3-D results over the 80 energy-group structure is computed as a function of the characteristic dimension and is shown in Figure 17. For reference, an example plot comparing the 1-D and 3-D results for the box geometry at 1 cm characteristic dimension (where the error is highest) is shown in Figure 18. There is excellent agreement between the models (less than 5% error) for object sizes greater than a few centimeters except for the slab configuration C geometry, which may not be appropriate to model in 1-D. The error at small dimensions stems from the high error in k_{eff}, on which the multiplication factor is based. Again, the error in the cylindrical geometry is consistently low for all object sizes.

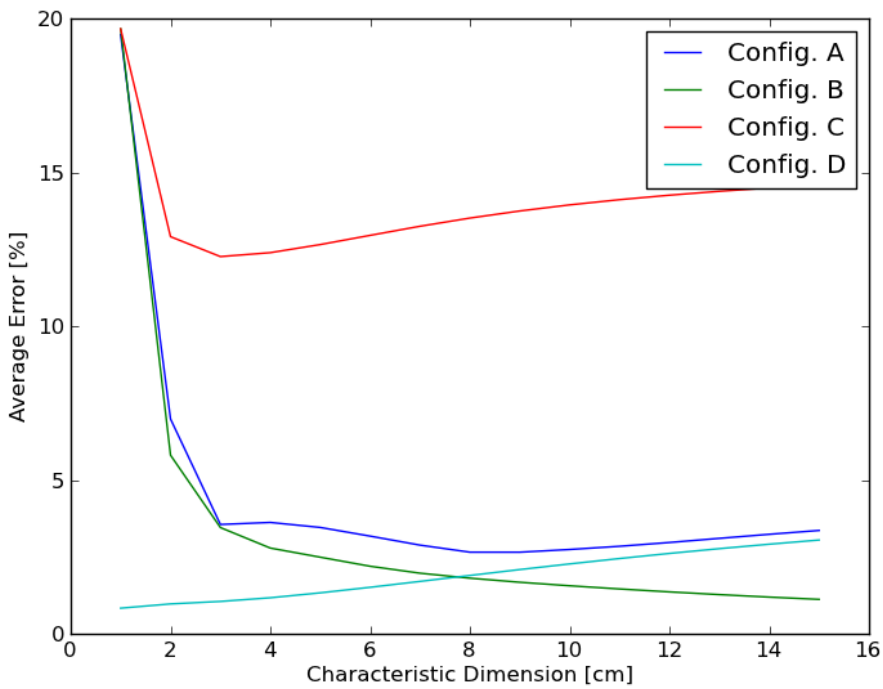

Figure 17. Average Error of Leakage Current between 1-D and Full-Dimensional Deterministic Models

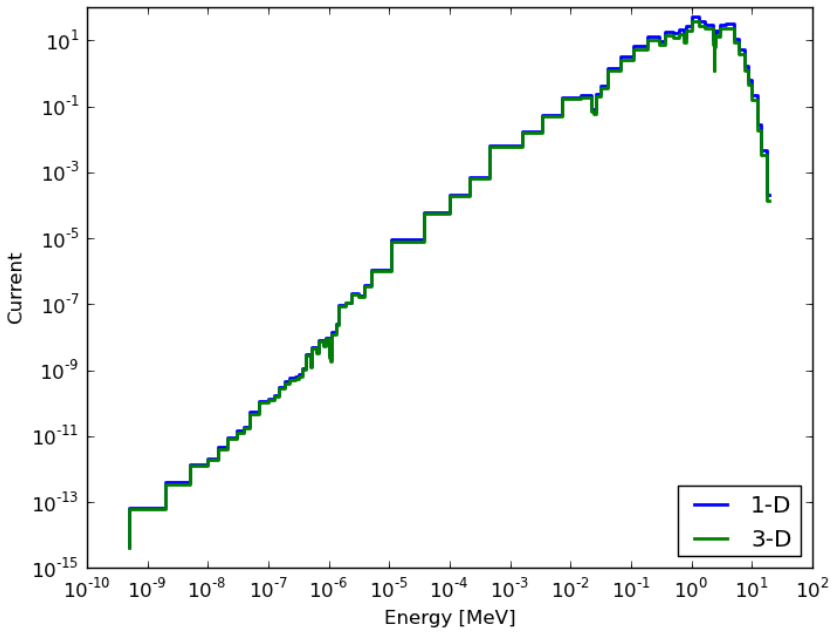

Figure 18. Comparison of Leakage Current Computed by 1-D and 3-D Deterministic Models for a 15 cm Box

3.1.3 Photon Leakage

Because ONELD is only a 1-D code, the leakage current out the front face as computed by ONELD is compared to results produced from MCNPX. The average error in the photon leakage spectrum is shown in Figure 19. Although the error may seem high compared to the neutron leakage, there is systematic error introduced by comparing the 1-D deterministic code to a 3-D Monte Carlo code. For example, the cross-sections in ONELD are collapsed into a 100-group structure based on empirical cross-section data, while MCNPX uses point-wise cross-sections. The important point is that the error is relatively constant over the characteristic dimensions as compared to the neutron leakage error, which is a strong function of dimension. This independence further strengthens the point made earlier that the photon leakage is not as dependent on the buckling correction.

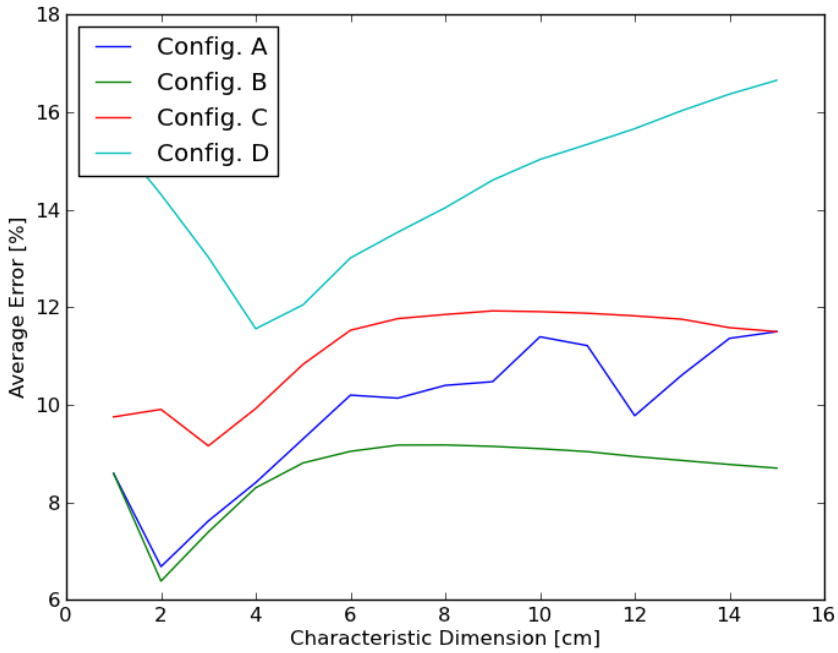

Figure 19. Average Error in Photon Leakage Current for Various Geometries Using the 1-D Approximation

3.1.4 Multi-Layered Geometries

When analyzing geometries with material layers present in the transverse directions, using the physical size of the object as the buckling height and width in 1-D simulations is not appropriate. For example, a cube of HEU embedded in a larger cube of polyethylene (PE) has material changes in all three Cartesian directions. Using the physical dimensions of the PE cube as the buckling width and height is equivalent to making a slab of HEU with those same dimensions, larger than the actual HEU slab, overestimating the multiplication of the system. Alternatively, the dimensions of the HEU cube may be used as the buckling width and height; this, however, will underestimate the criticality.

To demonstrate this effect, a toy HEU model is simulated. The model is a slab of HEU 10 cm wide, 30 cm tall, and 5 cm thick. It is completely surrounded on all sides (in three directions) by a 2 mm layer of steel followed by a 4 cm layer of polyethylene and 1 cm of lead. Thus, the physical size of the object is 10.2 cm x 15.2 cm x 35.2 cm. This is modeled using the physical dimensions of the object for the buckling height and width, and the dimensions of the HEU slab for the height and width. The 1-D results are compared to 3-D results in Table 1. The computed leakage currents are shown in Figure 20 and Figure 21. Even with the better agreement achieved using the transverse dimension of the fissile layer, the error incurred may be large depending on the shape of this layer. Multi-layered geometries are not well represented using the 1-D approximations. In such cases it is usually best to use a spherical representation of the model, unless the layers in the transverse directions are thin relative to the layers in the primary 1-D coordinate.

Table 1. Comparison of keff and Leakage Current Error for 3-D and 1-D Simulations

	Using Physical Height/Width		Using HEU Height/Width	
3-D k_{eff}	1-D k_{eff}	Average Current Error	1-D k_{eff}	Average Current Error
0.815	0.999	29 %	0.790	11%

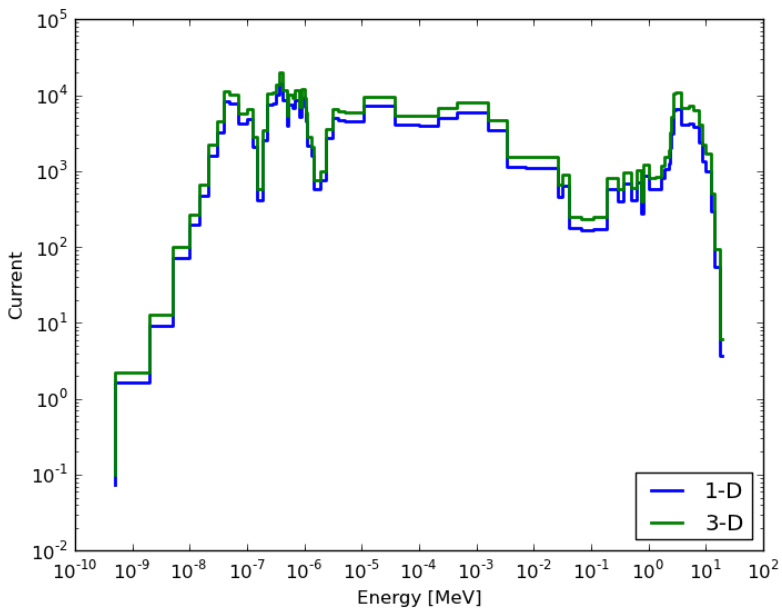

Figure 20. Simulated Leakage Current from 1-D and 3-D Models Assuming Physical Dimensions of the Object for the Buckling Height and Width

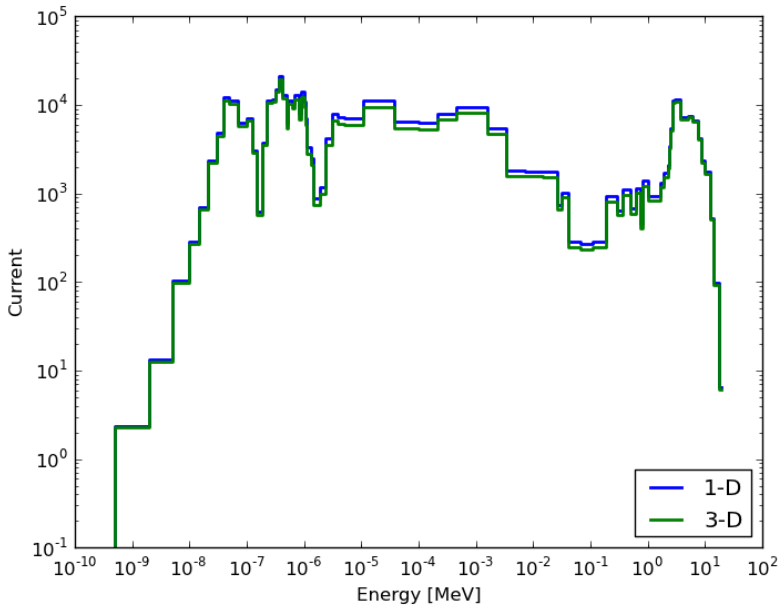

Figure 21. Simulated Leakage Current from 1-D and 3-D Models Assuming Dimensions of the HEU Slab for the Buckling Height and Width

Better agreement between the 1-D and 3-D simulations is achieved if the dimensions of the HEU material are used as the buckling height and width. Although the average current error is still high at around 11%, the computation time required for the 3-D simulation was 3400 seconds on a 3.3 GHz single processor compared to 1.7 seconds for the 1-D simulation.

3.2 Comparison to Experimental Data

A series of measurements were taken with an 85% high-purity germanium (HPGe) detector using an HEU plate, DU plate, and neptunium-237 cylinder as the source. The HEU plate is square with side length 4.17 inches and 0.085 inches thick with a mass of 446 grams. The DU plate is a double-stacked plate with length also 4.17 inches, 0.17 inches thick total with a total mass of 951 grams. The neptunium is contained in a stainless steel cylinder that is 0.75 inches outer diameter and 0.75 inches in total height. The total mass of neptunium is estimated to be 111 grams. The DU and HEU were measured at 2 meters while the neptunium was measured at 3 meters to reduce detector dead time.

These geometries are inherently multi-dimensional. The ability of GADRAS to model these geometries using the one-dimensional buckling approximation is compared against MCNPX and against the measured data. To remove any dependence on the source terms generated by GADRAS, the MCNPX source terms are computed with both RadSrc [4] and for comparison the GADRAS source terms. RadSrc computes the discrete gamma lines for any radioactive element mixture with proton number greater than lead, as well as an estimate on the bremsstrahlung continuum for U-238 chain radionuclides. The leakage current from the side of each object as computed by GADRAS and MCNPX is compared in Figure 22 through Figure 24. The coarse

energy group structure shown is not representative of the spectroscopic capabilities of GADRAS, as the leakage current from discrete gamma energies is computed separately by ray tracing.

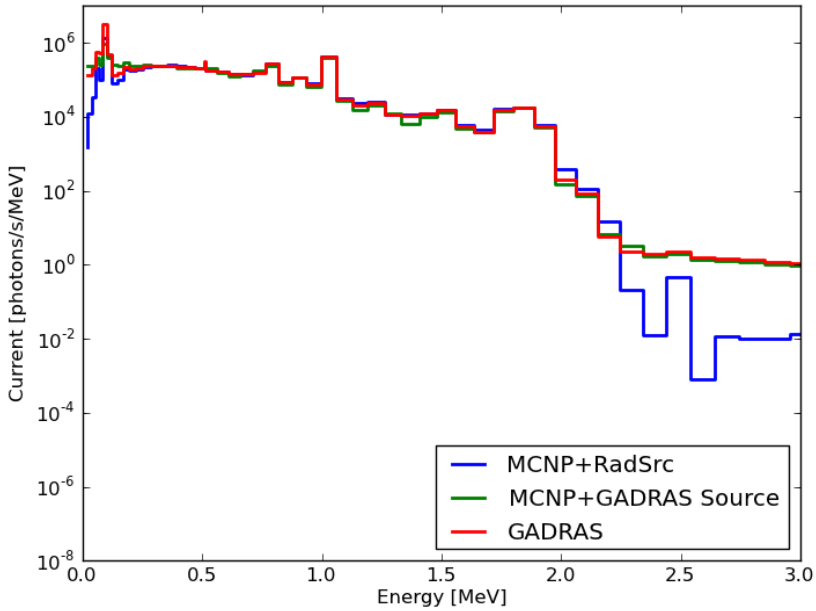

Figure 22. Simulated Photon Leakage Current from DU Plate

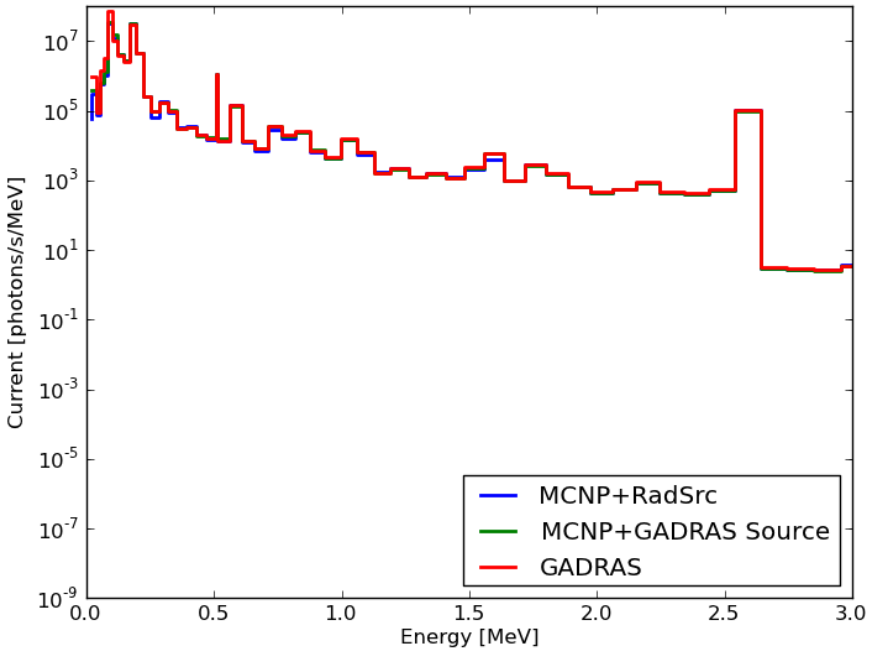

Figure 23. Simulated Photon Leakage Current from HEU Plate

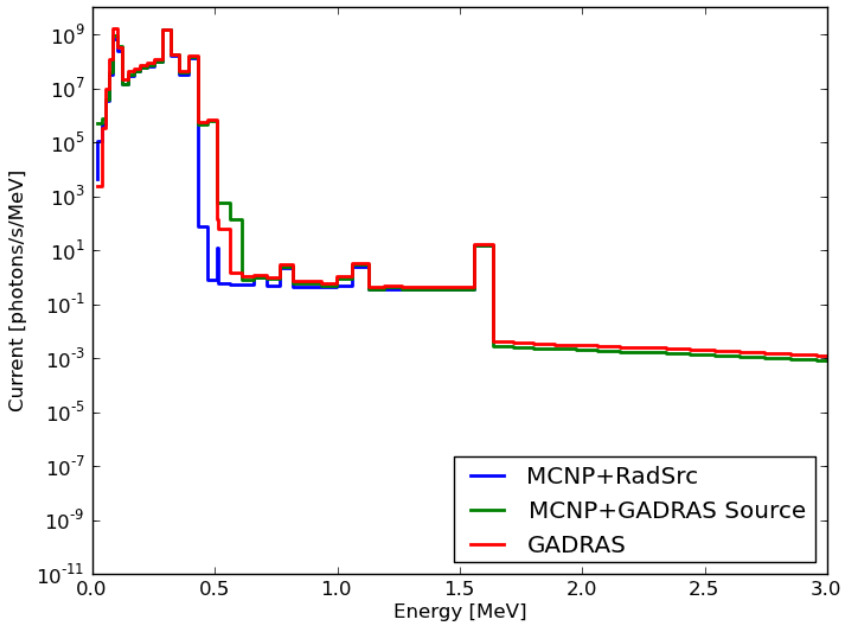

Figure 24. Simulated Photon Leakage Current from Neptunium Cylinder

Overall, the 1-D simulations from GADRAS with the buckling approximation compare well to the 3-D MCNPX simulations. The major discrepancies occur at higher energies (> 3 MeV), and around 500 keV with the neptunium cylinder. The higher energy discrepancy stems from RadSrc not computing the prompt photons from spontaneous fission, which is a continuous source that extends to high energies. The difference at around 500 keV with neptunium is from GADRAS utilizing a photon source database which has additional energies not specified in evaluated nuclear structure data file (ENSDF), on which the RadSrc calculation is based. Despite these differences, the overall agreement is good and confidence can be placed in the GADRAS leakage calculation and source terms.

As previously mentioned, GADRAS utilizes ray-tracing to compute the discrete uncollided photon leakage current, which comprise the photopeaks observed in detector signals. The buckling approximation and point-source-reduction approximations only apply to the group-averaged data. The ray-traced component is exact even for 3D geometries [5]. Combining the results from ray-trace and deterministic calculation for non-spherical geometries is a subject of ongoing research; however, preliminary results are promising. The experimental data is compared to the simulated results with and without ray-tracing in Figure 25 through Figure 27. The peaks from the deterministic simulations appear distorted or incorrect from the use of coarse energy groups.

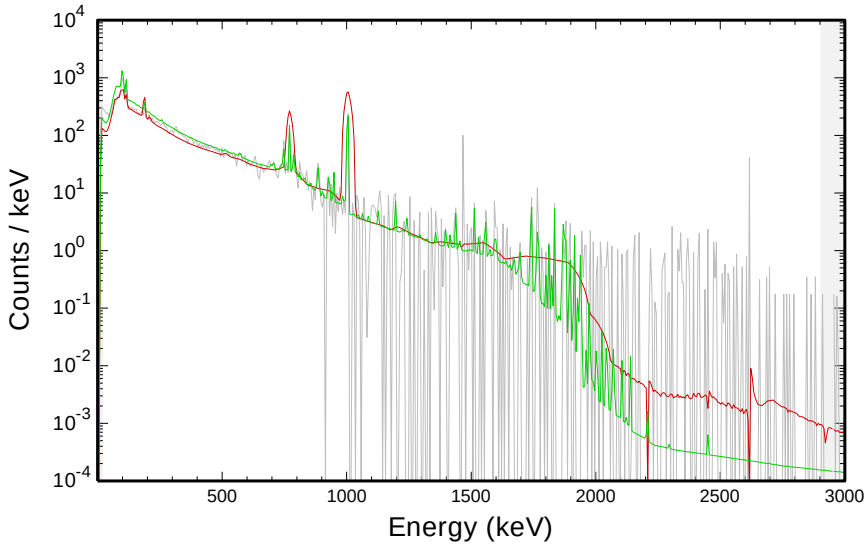

Figure 25. Comparison of Experimental (black), GADRAS-Simulated without Ray-tracing (red), and with Ray-tracing (green) HPGe Detector Signal from DU Plate

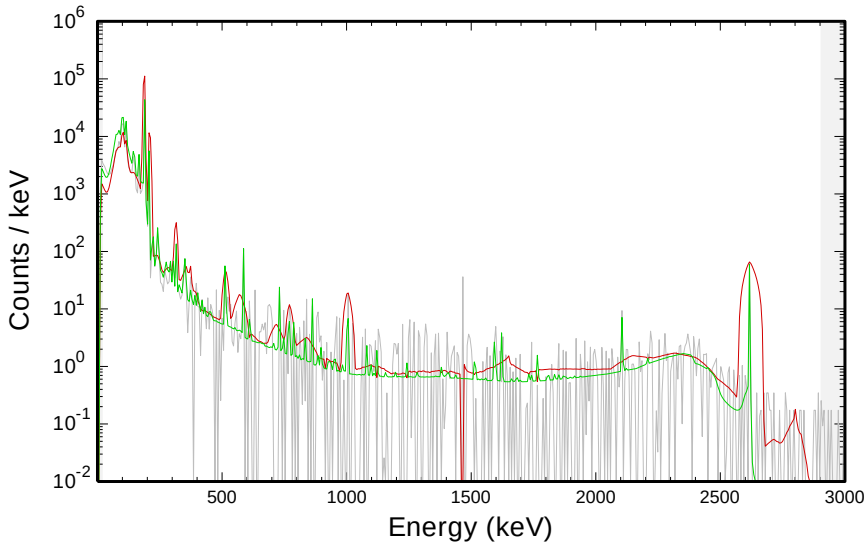

Figure 26. Comparison of Experimental (black), GADRAS-Simulated without Ray-tracing (red), and with Ray-tracing (green) HPGe Detector Signal from HEU Plate

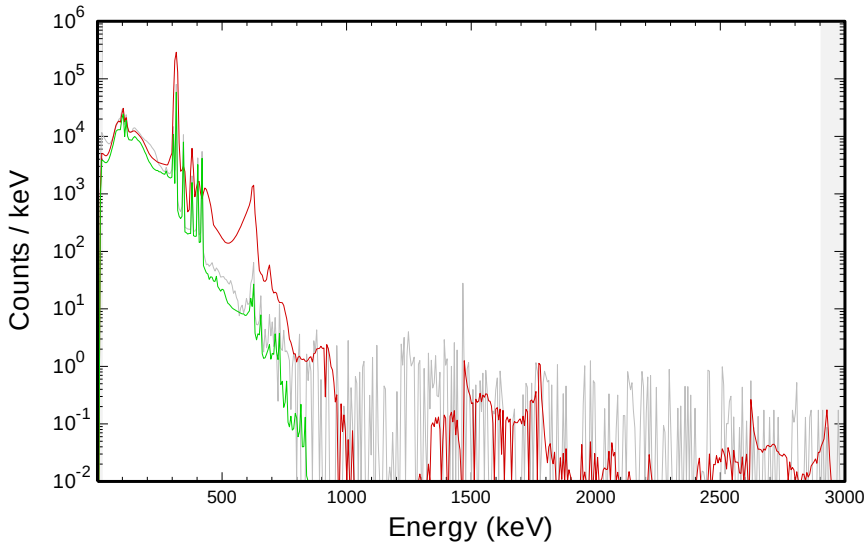

Figure 27. Comparison of Experimental (black), GADRAS-Simulated without Ray-tracing (red), and with Ray-tracing (green) HPGe Detector Signal from Neptunium Cylinder

The agreement between the simulated and experimental data is very good for the HEU and DU plates. However, the neptunium cylinder comparison without ray-tracing is much worse. Based on the good simulation agreement between the MCNPX and GADRAS leakage terms, the 1-D buckling approximation can be removed as a source of error. The agreement between the simulation with ray-tracing and the experiment indicates that the discrepancy may be caused by an error in the implementation of the point-source-reduction approximation. Unfortunately, this cylinder is the only experimental data currently available.

For comparison, the ability of all available geometries to approximate a spherical geometry experiment is also examined. The experiment measured the gamma signal from a 3 kg DU sphere using an HPGe detector. This sphere is simulated in GADRAS using a sphere, cylinder, and box. The cylinder height and diameter are made equal. The slab is made equal on all sides. The comparison between the experiment and simulated results, without the ray-traced component, are shown in Figure 28. The results are almost indistinguishable, giving credence to the methods studied and developed in this research.

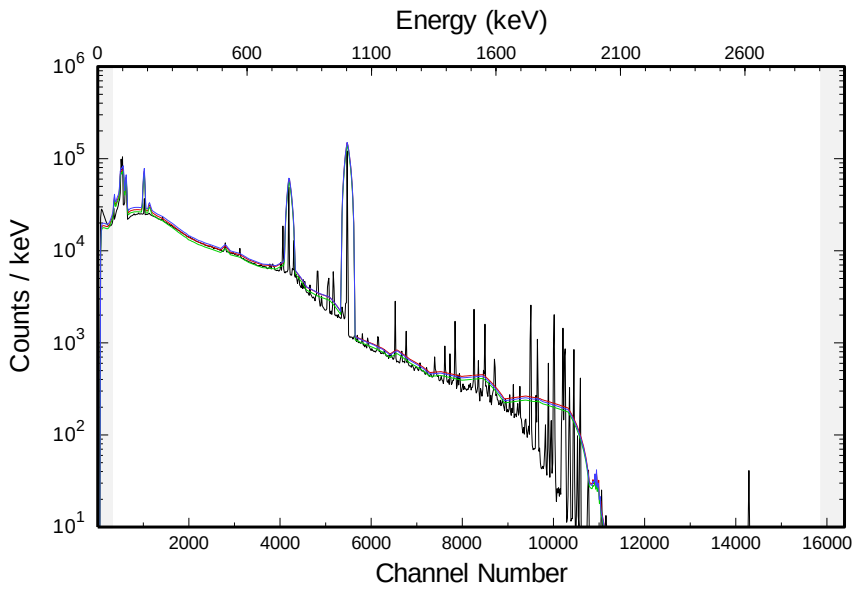

Figure 28. Comparison of Experimental (black), Simulated Sphere (red), Simulated Cylinder (green), and Simulated Slab (blue) for a 3 kg DU sphere measured with a HPGe detector

4 CONCLUSIONS

The ability to replicate results from 3-D radiation transport simulations utilizing approximate 1-D simulations was examined for HEU in a variety of geometries. For HEU placed in slab geometries with characteristic dimension greater than a few centimeters, the neutron leakage current computed by 3-D simulations may be replicated to within 5%, and k_{eff} to within 10% using the buckling correction approximation in 1-D. The leakage current and k_{eff} are approximated within 5% for the cylindrical geometry for all dimensions. However, the leakage in the transverse cylinder direction was fixed at 15 cm. The buckling approximation is never appropriate for simulating square-rod geometries where the x-dimension is along the length of the rod. It can be used to estimate the neutron leakage current with caution.

In general, the buckling correction appears to be valid and useful for objects where the transverse dimensions in which leakage is approximated are greater than a few centimeters. Related to this requirement is the mean-free-path of the fission neutrons, which is 2.8 cm in HEU. The built-in extrapolation distance used in PARTISN is most likely too large for these geometries in which the transverse dimensions are comparable to the mean-free-path of the neutron.

Geometries which are layered in two or more dimensions are also not appropriate for this approximation. For example, a cube of HEU embedded in a larger cube of polyethylene. The 1-D approximation requires uniformity in the traverse dimensions. Applying the dimensions of the polyethylene or HEU will result in an overestimation or underestimation of the multiplication.

The simulated data produced by GADRAS and MCNPX was also compared to a set of experiments performed on a DU plate, HEU plate, and neptunium cylinder. While the simulated results between GADRAS and MCNPX compared well for all three experiments, only the experimental results for the DU and HEU plates matched the simulations well. It is unknown at this time what the cause is for the discrepancy between the neptunium simulations and measurements.

4.1 Recommendations for GADRAS Users

1) Whenever possible, approximate the geometry using spherical shells.
2) Avoid modeling multi-layered geometries (e.g. cube within a cube or cylinder within a cylinder) using slabs or cylinders. Use spherical shells instead.
3) The length and width of a fissile slab, or the height of a fissile cylinder, should be at least a few centimeters.
4) The larger the length and width of the slab, the better the result.
5) The taller the height of the cylinder, the better the result.
6) Slab-geometry sources extend across the entire length and width of the slab. Thus, spherical sources shielded by a slab are better modeled by a sphere.
7) Cylindrical-geometry sources extend across the entire height of the cylinder. Spherical sources inside cylinders should be modeled as a sphere.
8) If using a cylinder, the detector should only be measuring the side of the cylinder, not the top or bottom.

9) If using a slab, the detector should be measuring either the large front or back face, not the other sides.
10) Table 2 contains a list of simple source and shielding configurations that will aid in selection of the appropriate model. The red areas indicate the distribution of the source or fissile material.

Table 2. Reference for Selecting Appropriate Geometry

When the actual geometry looks like:	Use:
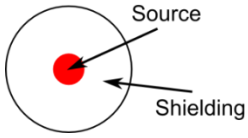	**Sphere**
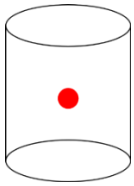	**Sphere**
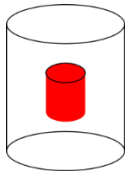	**Sphere**
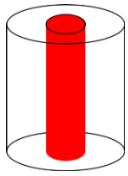	**Cylinder**
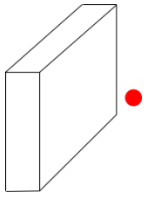	**Sphere**
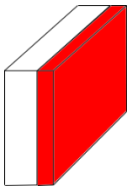	**Slab**
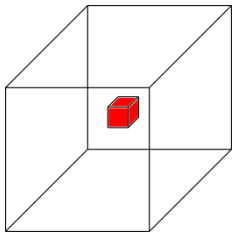	**Sphere**

5 REFERENCES

[1] R. E. Alcouffe et. al., *PARTISN: A Time-Dependent, Parallel Neutral Particle Transport Code System*, Los Alamos National Laboratory, LA-UR-08-07258.

[2] D.B. Pelowitz et. al., *MCNPX User's Manual Version 2.6.0*, Los Alamos National Laboratory, LA-CP-07-1473.

[3] L.J. Lorence et. al., *A User's Guide to CEPXS/ONELD Version 1.1*, Sandia National Laboratories, SAND91-1806.

[4] L. Hiller et. al., *RadSrc Library and Application Manual*, Lawrence Livermore National Laboratory, UCRL-TM-229497.

[5] D.J. Mitchell et. al., RayTrace3D in GADRAS Version 18.0, Sandia National Laboratories.

6 DISTRIBUTION

1	MS0782	Gregory G. Thoreson	ggthore@sandia.gov	06633
1	MS0782	Dean J. Mitchell	djmitch@sandia.gov	06633
1	MS0782	Lee T. Harding	lthard@sandia.gov	06633
1	MS0899	Technical Library	9536 (electronic copy)	

Sandia National Laboratories